Macromolecules

Article

pubs.acs.org/Macromolecules

Stimulus-Responsive Release from Poly(ferrocenylsilane) Nanocontainers

Laura Thomi, Philipp Schaefer, Katharina Landfester, and Frederik R. Wurm*

Max Planck Institute for Polymer Research, Ackermannweg 10, 55128 Mainz, Germany

Supporting Information

ABSTRACT: Redox-responsive poly(ferrocenylsilane) (PFS) is used to construct nanocontainers that can be loaded with hydrophobic cargo by a miniemulsion approach. The resulting structures comprise a solid shell surrounding a liquid oil core and have diameters of approximately 470 nm with a shell thickness of ca. 29 nm. The electrochemical behavior of the ferrocene group is investigated using cyclic voltammetry. Electrochemical oxidation and the thereby caused change of container morphology are shown. Hydrophobic molecules (Nile Red and 2-propylpyiridine) are loaded into the nanocontainers and can be released upon oxidation of the shell material. The oxidation is achieved chemically by the addition of hydrogen peroxide or by the enzymatic oxidation of glucose to release 2-propylpyridine over a period of time.

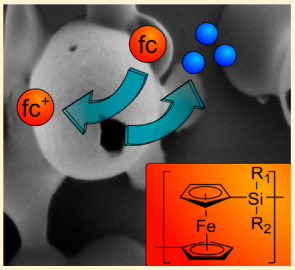

INTRODUCTION

Stimuli-responsive nanocontainers have the potential to be beneficial to a number of different fields, such as drug delivery, contrast agents, self-healing materials, the food sector, and containers for confined reactions.[1−6] Generally, the nanocontainer serves as protection for the cargo from external influences and can differ in size, shape, and composition. The next level is the introduction of responsive behavior, enabling the nanocontainer to react to an external stimulus. This opens up a field of functional nanocarriers able to interact with their environment in a predefined way. In most synthetic polymers, these stimuli are pH or temperature and sometimes light.[7−9] Some of the most common stimuli in nature, however, are oxidation and reduction processes, which occur for example in cellular signaling pathways and photosynthesis.[10−13] Man-made examples for such materials include the field of disulfide or diselenide chemistry, conductive polymers (e.g., polyaniline), or metallocenes (especially the ferrocene group (fc)).[4,14−20] Ferrocene itself is seldomly used; however, it can be incorporated into polymeric materials in either the side or main chain.[21] Poly(ferrocenylsilane)s (PFS), whose structure consists of alternating ferrocene and organosilane units, belong to the main chain ferrocene containing polymers. Among others, PFS materials have been studied regarding the self-assembly of block copolymers and subsequent use for the fabrication of magnetic ceramics.[22] The Vancso group investigated the formation of microcapsules through layer-by-layer self-assembly of polyanoinic and polycationic PFS.[23] The Manners group presented PFS microparticles, which were prepared *in situ* by a precipitation polymerization; also, the self-assembly in confinement of PFS-*b*-PS block copolymers was studied.[24,25]

Herein, we present the first preparation of stimulus-responsive PFS nanocontainers by a miniemulsion protocol that can be loaded with hydrophobic cargo, and their behavior upon chemical and electrochemical oxidation is studied. Oxidation of ferrocene (Fe^{2+}) to ferrocenium (Fe^{3+}) can be achieved by common oxidants, like H_2O_2, $KMnO_4$, or $FeCl_3$.[18,23] Additionally, we show that we show oxidation through the enzymatic oxidation of glucose by glucose oxidase. The oxidation process introduces a positive charge into the polymer backbone and enhances the swelling of the shell in water and the repulsion between the polymer chains. This generates a more permeable shell, which leads to an exchange between the core and the external water phase. With regard to the importance of redox processes in nature, these synthetic nanocontainers are an ideal handle to mimic biological systems. These redox-responsive PFS nanocarriers may find useful application in future sensing devices or self-healing matrices, where the redox potential of ferrocene triggers the release.

RESULTS AND DISCUSSION

PFS Nanocontainers: Preparation and Characterization. Redox-responsive nanocontainers based on a hydrophobic PFS block copolymer, namely poly(dimethylferrocenylsilane)$_{0.87}$-*block*-poly(methylvinylferrocenylsilane)$_{0.13}$ (hence referred to as PFS) (Figure S1 and Table S1), were prepared by a miniemulsion/solvent evaporation protocol (Figure 1a).[18] PFS was dissolved in dichloromethane (DCM) and dispersed in an aqueous solution of sodium dodecyl sulfate (0.01 wt %) (SDS). The DCM droplets were further stabilized by the addition of hexadecane, which acts as an ultrahydrophobe to reduce Ostwald ripening (i.e., the growth of larger colloidal structures at the expense of smaller ones).[26] In addition, as a nonsolvent for PFS, hexadecane serves as the oily core of the resulting nanocontainers. Stable DCM nanodroplets were achieved using ultrasonication. Subsequently, the DCM, a good solvent for PFS, is slowly evaporated. As the good solvent leaves the

Received: October 30, 2015
Revised: December 11, 2015
Published: December 22, 2015

DOI: 10.1021/acs.macromol.5b02367
Macromolecules 2016, 49, 105−109

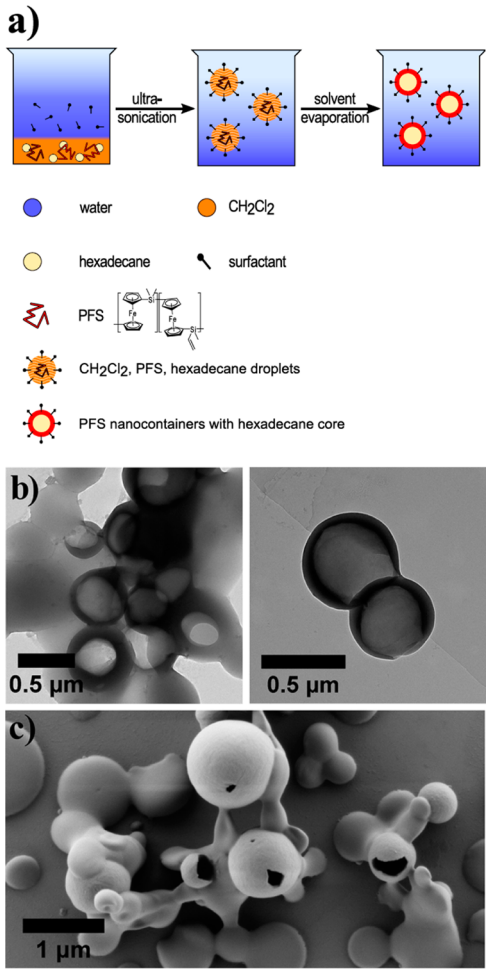

Figure 1. (a) Preparation of core−shell PFS nanocontainers through a miniemulsion/solvent evaporation protocol. (b) TEM images of PFS nanocontainers. (c) SEM image of PFS nanocontainers.

system, PFS is forced to precipitate at the interphase between the continuous water phase and the hexadecane core, thereby forming a solid shell around the liquid hexadecane core. This is possible because the interfacial tension between PFS and water is smaller than in a comparable hexadecane and water interface.[27] Therefore, a nanocontainer with PFS on the outside and hexadecane on the inside is energetically more favorable than vice versa. Afterward, the excess of free surfactant was removed by centrifugation of the nanocontainers. The supernatant, containing free surfactant, was removed, and the nanocontainers were redispersed in water. PFS nanocontainers with a mean hydrodynamic radius R_H of 233 ± 24 nm (determined by DLS) were generated by this protocol. Loading of these nanocontainers is possible with any hydrophobic cargo that does not interrupt the phase separation process.

The PFS nanocontainers were visualized by TEM and SEM (Figure 1b,c). They can be imaged without further staining due to the high electron density of the ferrocene group. The mean size from electron microscopy (506 nm) is in good accordance with the diameter obtained from DLS (466 nm). Their shell thickness can be estimated from TEM to be ca. 29 nm. The nanocontainers show an even surface morphology and high structural integrity; most retain their shape during the drying and imaging process. Differential scanning calorimetry (DSC) was used to assess the thermal properties of the nanocontainers. They exhibit a melting temperature T_m of 132 °C and a glass transition temperature T_g of 18 °C. The polymeric starting material shows similar results, a T_m of 129 °C and a T_g of 29 °C. Differences can be attributed to the surfactant as well as the hexadecane which both may act as a softener in the nanocontainers. This is in accordance with the properties expected of mainly symmetrically substituted PFS as well as DSC data in the literature.[28−30]

PFS Nanocontainers: Electrolysis. The redox-responsiveness of PFS nanocontainers was investigated using cyclic voltammetry (CV) (Figure 2). The redox behavior of the aqueous dispersion was compared to the polymeric starting material. The measurement of the polymeric starting material required the deposition of a thin PFS film on the working electrode because of the nonsolubility of the herein used PFS in water. The nanocontainers were measured either from drop-casting the dispersion on the electrode and obtaining a dried film or directly from dispersion (the numerical results are summarized in Table S2). The cyclic voltammogram of the adsorbed polymeric starting material film ("PFS ads." in Figure 2) shows a single pair of oxidation and reduction peaks with an anodic peak potential E_{pa} of 0.65 V and a cathodic peak potential E_{pc} of 0.50 V (see Figure S4 for a definition of E_p and I_p). It is known in the literature that cyclic voltammograms of PFS generally show two sets of oxidation and reduction peaks, which is attributed to the stepwise reversible oxidation of the ferrocene units along polymer chain. The first set of peaks is caused by oxidation of the chain at every other ferrocene unit. Subsequent oxidation of the remaining units is energetically less favorable and therefore shifted to a higher potential, giving rise to a second set of peaks.[31] However, this effect has been shown to be dependent on the solvent. In a solvent that does not facilitate swelling of the polymer film, interaction between the ferrocene centers and diffusion of counterions needed to balance the oxidation is hindered. Therefore, in solvents such as water the double peaks are rarely observable for hydrophobic PFS.[32] The peak separation ΔE_p and peak current I_p are indicators for the reversibility of a redox process. With ΔE_p of 0.15 V and almost identical I_{pc} and I_{pa}, the process is partly reversible.

The adsorbed PFS nanocontainers show an E_{pa} of 0.55 V and a E_{pc} of 0.52 V. The ΔE_p of 0.03 V is indicative of a reversible process. It is clear that the nanocontainer film differs in its electrochemical behavior from the polymer film. The adsorbed PFS film displays a large ΔE_p (0.15 V) as well as broad oxidation and reduction peaks, indicative of materials in which the charge transfer is hindered by diffusion. On the other hand, the adsorbed PFS nanocontainers show a small ΔE_p (0.03 V) and sharp oxidation and reduction peaks, typical for thin polymer films under non-diffusion-limited conditions.[33] We believe the explanation for this lies in the difference of chain mobility in the two species. The presence of softeners (i.e., SDS and hexadecane) in the adsorbed PFS nanocontainers lowers the T_g under room temperature (18 °C), while the adsorbed PFS film remains at a T_g above room temperature (29 °C). That means under the experimental conditions (ca. 20 °C) the PFS film is in a glassy state, while the PFS nanocontainers remain flexible, removing the diffusion barrier. We were also able to measure the redox behavior of the nanocontainers in dispersion. It was noticeable that the peak current of the dispersion was significantly smaller. This is caused by the reduced concentration near the electrode. The dispersion did

DOI: 10.1021/acs.macromol.5b02367
Macromolecules 2016, 49, 105−109

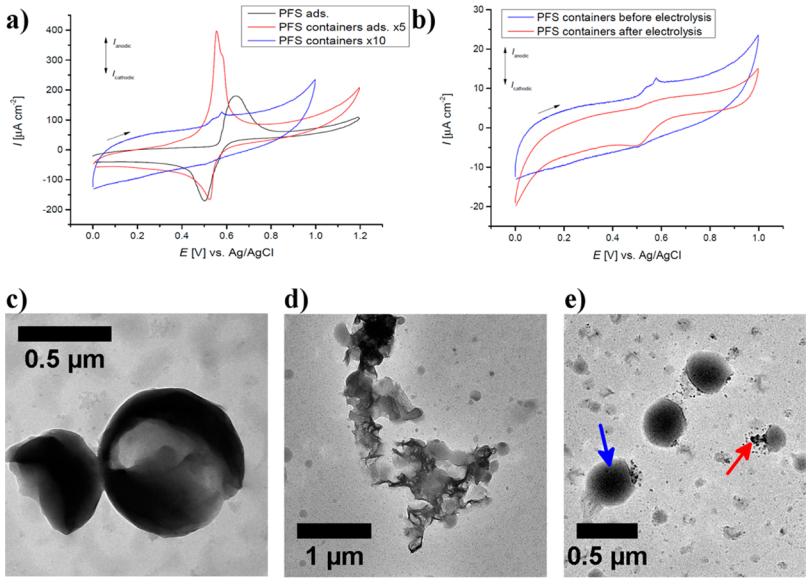

Figure 2. Electrolysis of PFS nanocontainers. (a) Cyclic voltammograms of PFS adsorbed on the electrode (black), PFS nanocontainers adsorbed on the electrode (red), and PFS nanocontainers in dispersion (blue). The latter two were multiplied by 5 and 10, respectively, for better visibility. Scan rates were 20 mV/s for PFS adsorbed and PFS nanocontainers adsorbed. PFS containers were measured at 10 mV/s. Measurements were carried out in PBS buffer. (b) Cyclic voltammograms of PFS nanocontainers before (blue) and after (red) electrolysis. Scan rates were 10 mV/s. Measurements were carried out in PBS buffer. (c) TEM image of PFS nanocontainers at 0% electrolysis. (d) TEM image of PFS nanocontainers at 50% electrolysis. (e) TEM image of PFS nanocontainers at 100% electrolysis.

not show a clear reduction peak, which could be caused by too little oxidized material being available near the electrode and the slow diffusion of the containers compared to lower molecular weight material. The dispersion exhibited an E_{pa} of 0.58 V and a E_{pc} of 0.50 V (as determined after electrolysis), similar values as obtained for the deposited nanocontainers.

In a next step the effect on electrochemical oxidation on the morphology of the nanocontainers was investigated. The oxidation of ferrocene is a one-electron process; therefore, the amount of ferrocene (n_{fc}) multiplied by the Faraday constant (F), i.e., the electric charge per mole electrons, equals the charge necessary for complete oxidation. A constant potential of 0.75 V—well above the oxidation potential of the nanocontainers—was applied until the electrolysis was complete. The CV measurements of the sample after electrolysis (Figure 2b) show almost no oxidation and a pronounced reduction peak, proving that the vast majority of the material was oxidized. The morphology of the containers was assessed at theoretically 0%, 50%, and 100% oxidation (Figure 2c–e) by TEM. At 0% oxidation the containers are intact, as to be expected. At 50% oxidation less intact core–shell structures can be detected. Instead, sharper fragmentation and high-contrast material appear. At 100% oxidation hexadecane droplets are visible (blue arrow in Figure 2e) with small high-contrast agglomerates next to them, presumably precipitated PFS (red arrow in Figure 2e) (drying effects during sample preparation have to be taken into account). TEM images are not representative of containers in solution, but it can be observed that their integrity decreases during electrolysis.

PFS Nanocontainers: Chemical Oxidation. In a next step, the oxidation of PFS containers by chemical means was investigated regarding (a) the change of the barrier properties of the PFS shell, visualized by confocal laser scanning microscopy (CLSM) and fluorescence intensity, and (b) the release of a hydrophobic cargo molecule measured by UV/vis spectroscopy. Chemical oxidation of PFS nanocontainers was achieved by the addition of hydrogen peroxide to the dispersion under acidic conditions.[34] The nanocontainers were imaged using CLSM (Figure 3a,b). Fluorescein isothiocyanate–dextran (FITC-dextran) was added to the continuous water phase as a green fluorescent marker. Before oxidation, the nanocontainers are visible in the transmission image and appear as dark spots in the fluorescent channel. The PFS shell acts as an efficient barrier; FITC-dextran cannot pass through it. After oxidation, the nanocontainers are still visible in the transmission channel; however, the fluorescence is now evenly distributed. This shows that oxidation leads to opening of the shell, which is caused by the positive charges in the main chain, which are introduced through oxidation. They enhance swelling in water and lead to repulsion of the polymer chains, thus allowing the diffusion of the aqueous FITC-dextran solution into the interior of the nanocontainers.

In another experiment, nanocontainers loaded with Nile Red (NR) were subjected to chemical oxidation by hydrogen peroxide under acidic conditions (Figure 3c). NR is a well-known solvatochrome, which will hardly fluoresce at all in a hydrophilic environment and show good fluorescence in a hydrophobic environment.[35] Here, the hexadecane core of the nanocontainers will provide the hydrophobic environment for NR, while the aqueous, continuous phase will represent the hydrophilic environment. PFS nanocontainers with a hexadecane and NR core were prepared, and the fluorescent intensity was measured. After addition of the oxidant to the dispersion the fluorescence intensity was monitored. PFS nanocontainers without NR were measured as a control to eliminate any influence of scattering during the measurement. The empty nanocontainers showed no significant fluorescence over time, which remains unchanged in the presence of the oxidant (Figure 3c). NR-loaded nanocontainers show a slight increase in fluorescence over time, which could be caused by evaporation of solvent, although steps were taken to keep

DOI: 10.1021/acs.macromol.5b02367
Macromolecules 2016, 49, 105–109

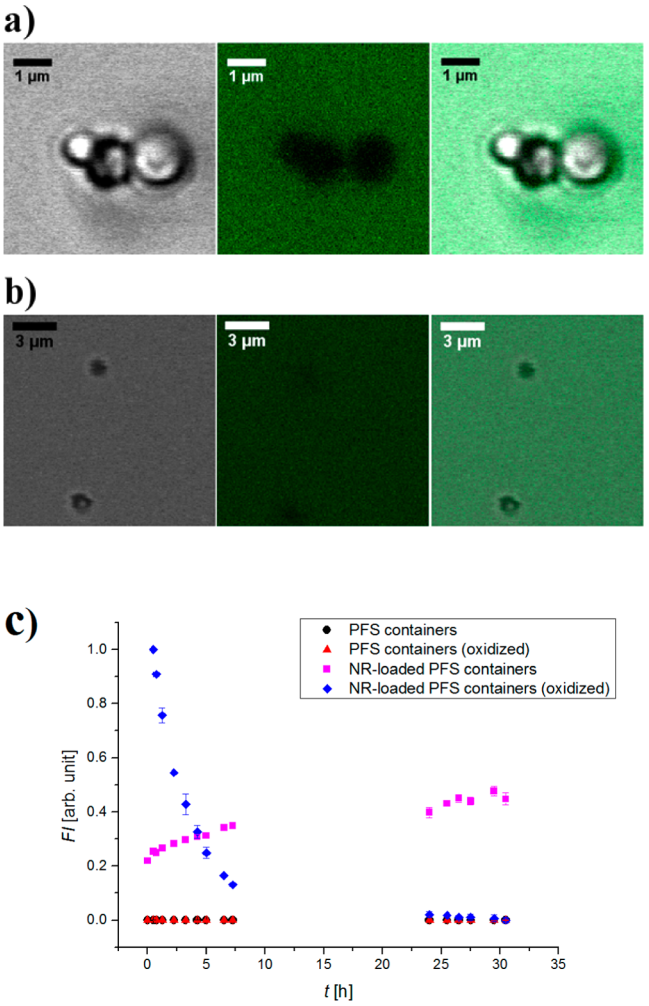

Figure 3. Confocal laser scanning microscopy (CLSM) images of PFS nanocontainers dispersed in FITC-dextran before (a) and after (b) oxidation with H_2O_2. Images show the transmission channel (left), fluorescent channel (middle), and the overlay (right). (c) Fluorescence intensity over time of PFS nanocontainers (black spheres), PFS nanocontainers with H_2O_2 (red triangles), Nile Red-loaded PFS nanocontainers (pink squares), and Nile Red-loaded PFS nanocontainers with H_2O_2 (blue diamonds). Error bars represent the mean of two separate measurements.

this to a minimum. However, the NR-loaded sample showed an unexpectedly high fluorescence at the start of the experiment, which decreased significantly over time. In control experiments it was found that hydrogen peroxide does not increase NR fluorescence (data not shown). The initially high fluorescence is thought to be caused by an instantaneous increase in container size upon oxidation. This is followed by an expansion of the oily core, reducing the self-quenching of NR molecules. It has been shown in the literature that the fluorescence of NR has a maximum at a certain concentration; once it is exceeded, quenching occurs.[36] After that, water can diffuse into the containers, and thus the fluorescence of NR decreases as the hydrophilicity of the environment increases.

Besides the chemical oxidation by the direct addition of hydrogen peroxide, the enzyme-triggered release from the PFS nanocontainers was investigated. The enzyme glucose oxidase (GOx) oxidizes glucose to D-glucono-δ-lactone and generates hydrogen peroxide continuously over time, providing less harsh conditions than adding the entire amount of hydrogen peroxide at the beginning (Scheme S1). In addition, release of a model compound was to be shown. 2-Propylpyridine was chosen for that as it is soluble in hexadecane, shows partial solubility in water, and is detectable using UV/vis spectroscopy. The PFS nanocontainer dispersion as well as the enzyme was placed inside a dialysis tube, which is permeable to the model compound and was dialyzed against an aqueous solution of glucose (1.32 wt %) and additional surfactant (0.01 wt % SDS) to prevent aggregation. The experiment was conducted under acidic conditions (0.56 wt % 0.1 M HCl). When 2-propylpyridine is released from the nanocontainers, it can diffuse through the dialysis tube into the outer phase. Aliquots were taken at defined points over time, in which 2-propylpyridine was detected using UV/vis spectroscopy. Figure 4 shows the release from PFS nanocontainers. The results

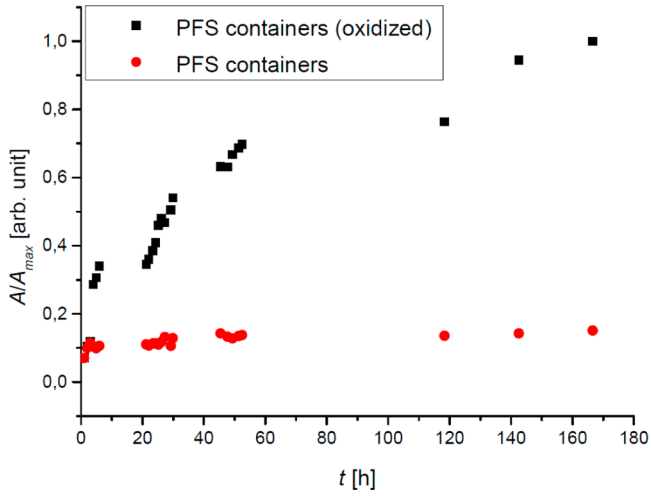

Figure 4. Release of 2-propylpyridine from PFS nanocontainers over time (red) and upon enzymatic oxidation with glucose oxidase in the presence of glucose (black).

clearly prove that the PFS nanocontainers can be oxidized by the enzymatically generated hydrogen peroxide and thus exhibits an enhanced release compared to the unoxidized nanocontainers, which show excellent barrier properties, also for 2-propylpyridine.

Thus, cargo release from PFS nanocontainers can be triggered using an enzymatically coupled reaction making these structures also interesting for biological applications.

CONCLUSION

In conclusion, the first redox-responsive poly(ferrocenylsilane) nanocontainers were prepared in a miniemulsion approach through solvent evaporation. Previously reported, related materials include PFS microcontainers by layer-by-layer assembly of polycationic and polyanionic PFS on colloidal templates and nanovesicles based on a hydrophilic PFS and a hydrophobic PDMS.[23,37] The obtained core−shell structures with a solid PFS shell and a liquid hexadecane core can be loaded with hydrophobic cargo. The nanocontainers exhibited diameters of ca. 466 nm determined from DLS. Electron microscopy (TEM and SEM) visualizes the core−shell structures, and an approximate shell thickness of 29 nm was determined. The preparation protocol allows loading the PFS nanocontainers with a great variety of hydrophobic molecules (Nile Red and 2-propylpyridine were used as examples). The

DOI: 10.1021/acs.macromol.5b02367
Macromolecules 2016, 49, 105−109

electrochemical behavior of PFS containers was studied using CV, where it was observed that the oxidation was less pronounced in dispersion and the reversibility of the process was hindered. However, complete oxidation was achieved through electrolysis, during which nanocontainer morphology change was studied using TEM. It was found that the nanocontainers did not retain their shape during the electrolysis and may release the cargo after an electrochemical trigger. Both the barrier properties of the PFS shell against leakage and permeation from outside were proven. However, after oxidation the permeation through the PFS barrier or the release from the core of the nanocontainers was proven. The release can also be coupled to the enzymatic oxidation of glucose with oxygen by the enzyme glucose oxidase. The pendant vinyl groups of the PFS block copolymer used in this work offer possibilities for future modification of the nanocontainers. The herein presented PFS nanocontainers add a new tool to the kit of responsive nanocarriers, enriching the field of smart materials and their application in drug delivery, self-healing applications, and synthetic biology.

■ ASSOCIATED CONTENT

Supporting Information

The Supporting Information is available free of charge on the ACS Publications website at DOI: 10.1021/acs.macromol.5b02367.

Experimental details and additional characterization data (PDF)

■ AUTHOR INFORMATION

Corresponding Author

*E-mail wurm@mpip-mainz.mpg.de (F.R.W.).

Funding

L.T., F.R.W., and K.L. thank the BMBF/MPG network MaxSynBio. F.R.W. and P.S. thank the Max Planck Graduate Center for support.

Notes

The authors declare no competing financial interest.

■ ACKNOWLEDGMENTS

The authors thank Gunnar Glasser for SEM measurements, Patricia Renz for CLSM assistance, and Petra Räder for DSC measurements.

■ REFERENCES

(1) Gao, X.; Cui, Y.; Levenson, R. M.; Chung, L. W. K.; Nie, S. *Nat. Biotechnol.* **2004**, *22* (8), 969−976.
(2) Savić, R.; Luo, L.; Eisenberg, A.; Maysinger, D. *Science* **2003**, *300* (5619), 615−618.
(3) Na, H. B.; Song, I. C.; Hyeon, T. *Adv. Mater.* **2009**, *21* (21), 2133−2148.
(4) Lv, L.-P.; Zhao, Y.; Vilbrandt, N.; Gallei, M.; Vimalanandan, A.; Rohwerder, M.; Landfester, K.; Crespy, D. *J. Am. Chem. Soc.* **2013**, *135* (38), 14198−14205.
(5) Ezhilarasi, P. N.; Karthik, P.; Chhanwal, N.; Anandharamakrishnan, C. *Food Bioprocess Technol.* **2013**, *6* (3), 628−647.
(6) Chen, Q.; Schönherr, H.; Vancso, G. J. *Small* **2009**, *5* (12), 1436−1445.
(7) Chen, G.; Hoffman, A. S. *Nature* **1995**, *373* (6509), 49−52.
(8) Tanaka, T. *Phys. Rev. Lett.* **1978**, *40* (12), 820−823.
(9) Irie, M. Stimuli-responsive poly(N-isopropylacrylamide). Photo- and chemical-induced phase transitions. In *Responsive Gels: Volume Transitions II*; Dušek, K., Ed.; Springer: Berlin, 1993; Vol. *110*, pp 49−65.
(10) Napoli, A.; Valentini, M.; Tirelli, N.; Muller, M.; Hubbell, J. A. *Nat. Mater.* **2004**, *3* (3), 183−189.
(11) Cerritelli, S.; Velluto, D.; Hubbell, J. A. *Biomacromolecules* **2007**, *8* (6), 1966−1972.
(12) Stamler, J. S. *Cell* **1994**, *78* (6), 931−936.
(13) Ciesielski, P. N.; Faulkner, C. J.; Irwin, M. T.; Gregory, J. M.; Tolk, N. H.; Cliffel, D. E.; Jennings, G. K. *Adv. Funct. Mater.* **2010**, *20* (23), 4048−4054.
(14) Liang, K.; Such, G. K.; Zhu, Z.; Yan, Y.; Lomas, H.; Caruso, F. *Adv. Mater.* **2011**, *23* (36), H273−H277.
(15) Bian, S.; Zheng, J.; Tang, X.; Yi, D.; Wang, Y.; Yang, W. *Chem. Mater.* **2015**, *27* (4), 1262−1268.
(16) Ma, N.; Li, Y.; Xu, H.; Wang, Z.; Zhang, X. *J. Am. Chem. Soc.* **2010**, *132* (2), 442−443.
(17) Cunningham, A. F. *J. Am. Chem. Soc.* **1991**, *113* (13), 4864−4870.
(18) Staff, R. H.; Gallei, M.; Mazurowski, M.; Rehahn, M.; Berger, R.; Landfester, K.; Crespy, D. *ACS Nano* **2012**, *6* (10), 9042−9049.
(19) Elbert, J.; Krohm, F.; Rüttiger, C.; Kienle, S.; Didzoleit, H.; Balzer, B. N.; Hugel, T.; Stühn, B.; Gallei, M.; Brunsen, A. *Adv. Funct. Mater.* **2014**, *24* (11), 1591−1601.
(20) Galloro, J.; Ginzburg, M.; Míguez, H.; Yang, S. M.; Coombs, N.; Safa-Sefat, A.; Greedan, J. E.; Manners, I.; Ozin, G. A. *Adv. Funct. Mater.* **2002**, *12* (5), 382−388.
(21) Natalello, A.; Alkan, A.; Friedel, A.; Lieberwirth, I.; Frey, H.; Wurm, F. R. *ACS Macro Lett.* **2013**, *2* (4), 313−316.
(22) Cao, L.; Massey, J. A.; Winnik, M. A.; Manners, I.; Riethmüller, S.; Banhart, F.; Spatz, J. P.; Möller, M. *Adv. Funct. Mater.* **2003**, *13* (4), 271−276.
(23) Ma, Y.; Dong, W.-F.; Hempenius, M. A.; Mohwald, H.; Julius Vancso, G. *Nat. Mater.* **2006**, *5* (9), 724−729.
(24) Kulbaba, K.; Cheng, A.; Bartole, A.; Greenberg, S.; Resendes, R.; Coombs, N.; Safa-Sefat, A.; Greedan, J. E.; Stöver, H. D. H.; Ozin, G. A.; Manners, I. *J. Am. Chem. Soc.* **2002**, *124* (42), 12522−12534.
(25) Arsenault, A. C.; Rider, D. A.; Tétreault, N.; Chen, J. I. L.; Coombs, N.; Ozin, G. A.; Manners, I. *J. Am. Chem. Soc.* **2005**, *127* (28), 9954−9955.
(26) Barrios, S. B.; Petry, J. F.; Weiss, C. K.; Petzhold, C. L.; Landfester, K. *J. Appl. Polym. Sci.* **2014**, *131* (15), 40569.
(27) Wu, D.; Hornof, V. *Chem. Eng. Commun.* **1999**, *172* (1), 85−106.
(28) Kulbaba, K.; Manners, I. *Macromol. Rapid Commun.* **2001**, *22* (10), 711−724.
(29) Gohy, J.-F.; Lohmeijer, B. G. G.; Alexeev, A.; Wang, X.-S.; Manners, I.; Winnik, M. A.; Schubert, U. S. *Chem. - Eur. J.* **2004**, *10* (17), 4315−4323.
(30) Gilroy, J. B.; Patra, S. K.; Mitchels, J. M.; Winnik, M. A.; Manners, I. *Angew. Chem., Int. Ed.* **2011**, *50* (26), 5851−5855.
(31) Wurm, F.; Hilf, S.; Frey, H. *Chem. - Eur. J.* **2009**, *15* (36), 9068−9077.
(32) Wang, X.-J.; Wang, L.; Wang, J.-J.; Chen, T. *Electrochim. Acta* **2007**, *52* (12), 3941−3949.
(33) Peerce, P. J.; Bard, A. J. *J. Electroanal. Chem. Interfacial Electrochem.* **1980**, *114* (1), 89−115.
(34) Fomin, F. M.; Zaitseva, K. S. *Russ. J. Phys. Chem.* **2014**, *88* (3), 466−470.
(35) Greenspan, P.; Mayer, E. P.; Fowler, S. D. *J. Cell Biol.* **1985**, *100* (3), 965−973.
(36) Chen, W.; Zhang, C.; Song, L.; Sommerfeld, M.; Hu, Q. *J. Microbiol. Methods* **2009**, *77* (1), 41−47.
(37) Power-Billard, K. N.; Spontak, R. J.; Manners, I. *Angew. Chem., Int. Ed.* **2004**, *43* (10), 1260−1264.

DOI: 10.1021/acs.macromol.5b02367
Macromolecules 2016, 49, 105−109